Harnessing Oxidized Amines as Robust Sorbents for Carbon Capture

Authors: Sijing Meng[1], Tristan H. Lambert[1*], Phillip J. Milner[1*]

Affiliations:

[1] Department of Chemistry and Chemical Biology, Cornell University; Ithaca, New York 14850, United States.

*Corresponding authors. Email: Tristan H. Lambert. thl36@cornell.edu, Phillip J. Milner. pjm347@cornell.edu.

Abstract

Carbon capture and sequestration (CCS) is imperative to mitigating climate change[1]. Aqueous amine solutions are the leading technology for CO_2 separations[2], but they suffer from chemical instability under scrubbing conditions, corrosiveness, and toxicity, hindering their long-term deployment[3–5]. Herein, we demonstrate that tertiary amine *N*-oxides, an oxidative degradation product of amines[6,7], can remove CO_2 from dilute streams, including flue gas from a natural gas-fired power plant. Extensive spectroscopic and computational studies support that the non-toxic, non-corrosive, and inexpensive 4-methylmorpholine *N*-oxide (MMNO) captures CO_2 under humid conditions via the formation of a hydrogen-bond-stabilized bicarbonate (HCO_3^-) species, despite being significantly less basic than an amine. MMNO exhibits improved oxidative and thermal stability compared to structurally similar amines, highlighting the potential of *N*-oxides to complement traditional amine-based scrubbers for industrial carbon capture applications.

Main

Following current trends in greenhouse gas emissions, the average temperature of the Earth's surface will inevitably warm by 1.5 °C, the global limit agreed to under the 2015 Paris Agreement[8], by as early as 2034[9]. Due to this urgent situation, carbon capture and sequestration (CCS) from fossil fuel-fired power plants and relative hard-to-abate sectors plays a key role during clean energy transition to reach international climate targets. Although global CCS deployment has bloomed in recent years to reach a capacity of ~50 Mt CO_2 captured and stored annually[10,11], this amount only accounts for 0.6% of the value needed (>8 Gt) to achieve net zero CO_2 emissions, consistent with the Paris Agreement 1.5 °C limit, by 2050[12,13] (Fig. 1a). Clearly, this disparity requires a large expansion of CCS deployment worldwide to meet the climate mitigation targets over the coming decades.

Since their conception nearly a century ago[14], aqueous amine scrubbers have emerged as the most technology-ready system for CCS[2]. The first-generation technology using monoethanolamine (MEA) and later advances using secondary/tertiary amines demonstrate high selectivity for CO_2 via reversible ammonium carbamate formation under dry conditions and ammonium bicarbonate (HCO_3^-) and/or carbonate (CO_3^{2-}) formation under humid conditions (Fig. 1a)[15]. However, amines suffer from several critical drawbacks that hinder their widespread deployment. First, high

regeneration temperatures (>100 °C) in temperature-swing processes are needed to reverse the strong binding of CO_2 ($-\Delta H_{abs} > 12$ kcal/mol)[16], which accounts for 70–80%[17,18] of the total energy cost required to continuously operate a scrubber. Second, high operation temperatures and the presence of oxygen combined with leached metal ions lead to significant thermal and oxidative amine degradation into over 100 reported products, necessitating continuous replacement and complex reclaiming processes[3,18–22]. The decomposition of amines, which is hard to avoid due to their highly electron-rich, nucleophilic, and basic nature, adds an additional 10% to the overall cost of carbon capture systems[23]. Last, amines are toxic, volatile, and corrosive, which presents challenges regarding their safe handling on multi-ton scale[4,5,24,25]. As such, replacements for amines that maintain their reactivity-based selectivity for CO_2 while also demonstrating improved stability and reduced energy use, corrosiveness, volatility, and toxicity, would greatly accelerate the global adoption of CCS.

One type of reported oxidation products of tertiary amines are the corresponding trialkylamine *N*-oxides[6,7] (Fig. 1b). The formation of *N*-oxides would normally be considered a dead-end for carbon capture due to the loss of the nucleophilic and basic nitrogen center. Nonetheless, *N*-oxides are highly prevalent in both biological and industrial settings for a variety of applications, as they are generally non-toxic and non-corrosive[26–28]. For example, trimethyl amine *N*-oxide (TMAO) is found in deep-sea organisms as an osmolyte to prevent denaturation of vital proteins[29,30]. Small-molecule *N*-oxides, specifically *N*-methylmorpholine *N*-oxide (MMNO), are used industrially in the Lyocell process to dissolve cellulose[31–34]. Long-chain and polymeric *N*-oxides are used as surfactants in cleansing products such as detergents and shampoos, and industrially as antifouling reagents and kinetic hydrate inhibitors[26,35,36].

Herein, we demonstrate that oxidation of trialkylamines to the corresponding trialkylamine *N*-oxides does not preclude their use for carbon capture, as weakly basic MMNO is still capable of binding CO_2 under humid conditions via the formation of a hydrogen-bond-stabilized HCO_3^- species (Fig. 1c). Unlike amines, MMNO exhibits good oxidative and thermal stability, is minimally volatile[37], and binds CO_2 weakly enough to allow for facile release at room temperature in a simulated vacuum swing process and ~ 65 °C in a simulated temperature swing process. Along with their similar structural tunability to amines, these promising features suggest that trialkylamine *N*-oxides such as MMNO may serve as industrially viable alternative for amines with improved longevity and reduced operating costs.

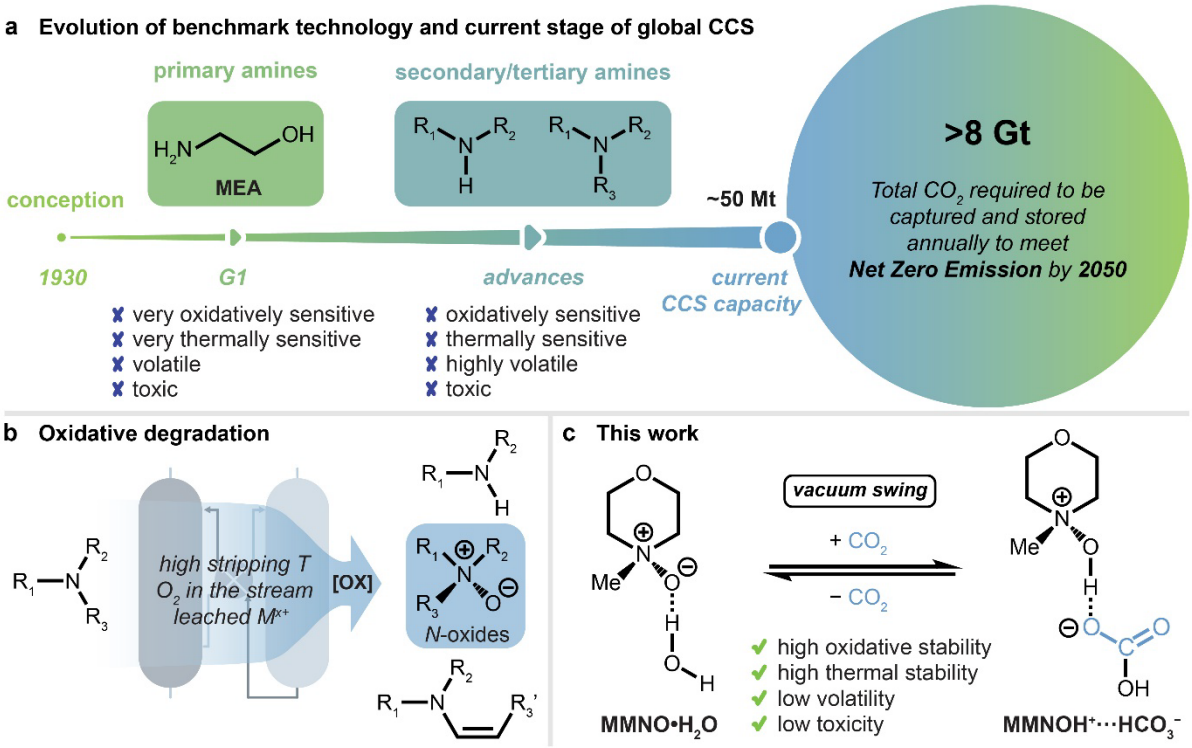

Fig. 1. Evolution and challenges of carbon capture and sequestration (CCS) | a, Evolution of amine-scrubbing technology from 1st generation (G1) monoethanolamine (MEA) to secondary/tertiary amines, and gap between current CCS capacities and required capacities. **b**, Oxidative instability limits the large-scale employment of amine-scrubbing technologies under industrially relevant conditions. **c**, CO_2 capture using 4-methylmorpholine *N*-oxide hydrate (this work).

Role of water in CO_2 capture with MMNO

To probe whether MMNO is capable of reversibly binding CO_2, ^{13}C nuclear magnetic resonance (NMR) experiments in wet deuterated dimethyl sulfoxide (DMSO-D_6) were conducted at 25 °C (Supplementary Fig. 3). The presence of MMNO induced significant broadening of the resonance corresponding to dissolved CO_2 (124–125 ppm, see Supplementary Fig. 5 for comparison with non-broadened resonances); in addition, a new broad resonance (158–159 ppm) corresponding to a carbonyl (C=O)-containing species was observed. The broad nature of the observed resonances indicates that free CO_2 and the new species are undergoing slow-intermediate exchange on the ^{13}C NMR time scale ($k_{ex} < |\Delta\nu|$)[38]. As such, experiments were conducted with $^{13}CO_2$ in anhydrous DMSO-D_6 to better visualize the chemically bound $^{13}CO_2$ adduct and to carefully control the equivalents of H_2O present in solution (Fig. 2a). With water or anhydrous MMNO alone, no new species form upon dosing the solution with $^{13}CO_2$. However, when an equimolar solution of H_2O and MMNO is dosed with $^{13}CO_2$, a broad new resonance appears at 158–159 ppm, which is assigned to a $^{13}CO_2$ adduct of MMNO and H_2O (MMNO•H_2O•$^{13}CO_2$) containing a C=O group (the same is observed for up to 20 equivalents of H_2O, see Fig. 2a, 3a, and Supplementary Fig. 13). The free $^{13}CO_2$ resonance is also significantly broadened due to chemical exchange interactions (Fig. 2a). Notably, bubbling N_2 through the solution for 60 minutes at room temperature

(simulating a vacuum swing) leads to full desorption of chemically bound $^{13}CO_2$, supporting that the reaction between MMNO, H_2O, and $^{13}CO_2$ can be readily reversed (Fig. 2a). No degradation or rearrangement of MMNO occurred under these conditions, as confirmed by $^{1}H–^{13}C$ 2D HMBC spectroscopy (Supplementary Fig. 39). Notably, CO_2 could also be released at ~65 ° C in a simulated temperature swing process, reflecting the lower potential regeneration energy costs of MMNO compared to amines (Supplementary Fig. 29).

It is clear that the presence of H_2O is vital for MMNO to react with CO_2. Unlike amines, *N*-oxides are not strongly nucleophilic nor Brønsted basic (pK_a of R_3N^+–OH = 4.5–5), yet they are highly Lewis basic and one of the strongest neutral organic hydrogen-bond acceptors due to the polar N→O bond (dipole moment ~5 D) and the formal negative charge on O[26,39]. To better understand the role of H_2O in the CO_2 capture process, MMNO hydrate (MMNO•$(H_2O)_n$) formation was first probed using the interaction-induced chemical shift perturbations of MMNO as the host and H_2O as the guest molecule in DMSO-D_6. NMR titration experiments were performed with three different MMNO concentrations (0.125 M, 0.25 M, and 0.5 M) with increasing equivalents of water. At all three host concentrations, the ^{1}H chemical shifts were perturbed as H_2O was titrated (Fig. 2b, Supplementary Figs. 6, 8, and 10; see Equation 1 in Supplementary Information), consistent with fast-exchange interactions between MMNO and its hydrates on the ^{1}H NMR time scale ($k_{ex} >> |\Delta\nu|$) [38]. Among the nuclei monitored, H_a and H_d of MMNO experience the largest perturbations, indicating that they participate in the interaction with H_2O most closely. The NMR titration experimental data were fit to five binding models corresponding to host:guest ratios of 1:1 (monohydrate) or 1:2 (dihydrate) using Bindfit with a global non-linear regression method[40–42] (see Supplementary Information for theory, and Supplementary Table 1 for model features). The 1:2 full model yielded the best cov_{fit} (see Supplementary Table 1 for details), indicating that the binding of the second H_2O molecule is made weaker by the binding of the first, with an interaction parameter (α) of 0.2 (Equation 11 in Supplementary Information). Together, these NMR studies support the association of H_2O with MMNO to form both MMNO•H_2O and MMNO•$(H_2O)_2$, with the maximum relative molar ratio of MMNO•H_2O reached at 5–10 equivalents of H_2O added relative to MMNO (Fig. 3b).

Intermolecular 2D nuclear Overhauser effect spectroscopy (NOESY) experiments were conducted to further probe the nature of the interactions between H_2O and MMNO (Fig. 2c–d and Supplementary Figs. 20–21). With 1 equivalent of H_2O in 0.25 M MMNO in DMSO-D_6 at a long mixing time of 600 ms, the NOESY spectrum shows several major cross-peaks resulting from the close contact between the H_2O proton (3.6 ppm) and the methyl H_c (3.0 ppm) and α (to N)-equatorial H_d (2.7 ppm) protons of MMNO (Fig. 2c). This spectrum provides direct evidence for the preferred H_2O binding site (**A**) for MMNO•H_2O, in which H_2O hydrogen bonds to the oxygen of MMNO in an orientation pointing away from the ring. In contrast, with 20 equivalents of H_2O, an additional intense cross-peak becomes visible. The new peak represents an interaction between the H_2O proton (3.7 ppm) and β (to N)-axial H_a (4.0 ppm), revealing the second binding pocket (**B**) for water to hydrogen bond with MMNO in an orientation pointing towards the ring in

MMNO•$(H_2O)_2$ (Fig. 2d). Combining the NMR titration and NOESY experiments, the mechanism of MMNO hydrate and dihydrate formation can be recapitulated (Fig. 2e).

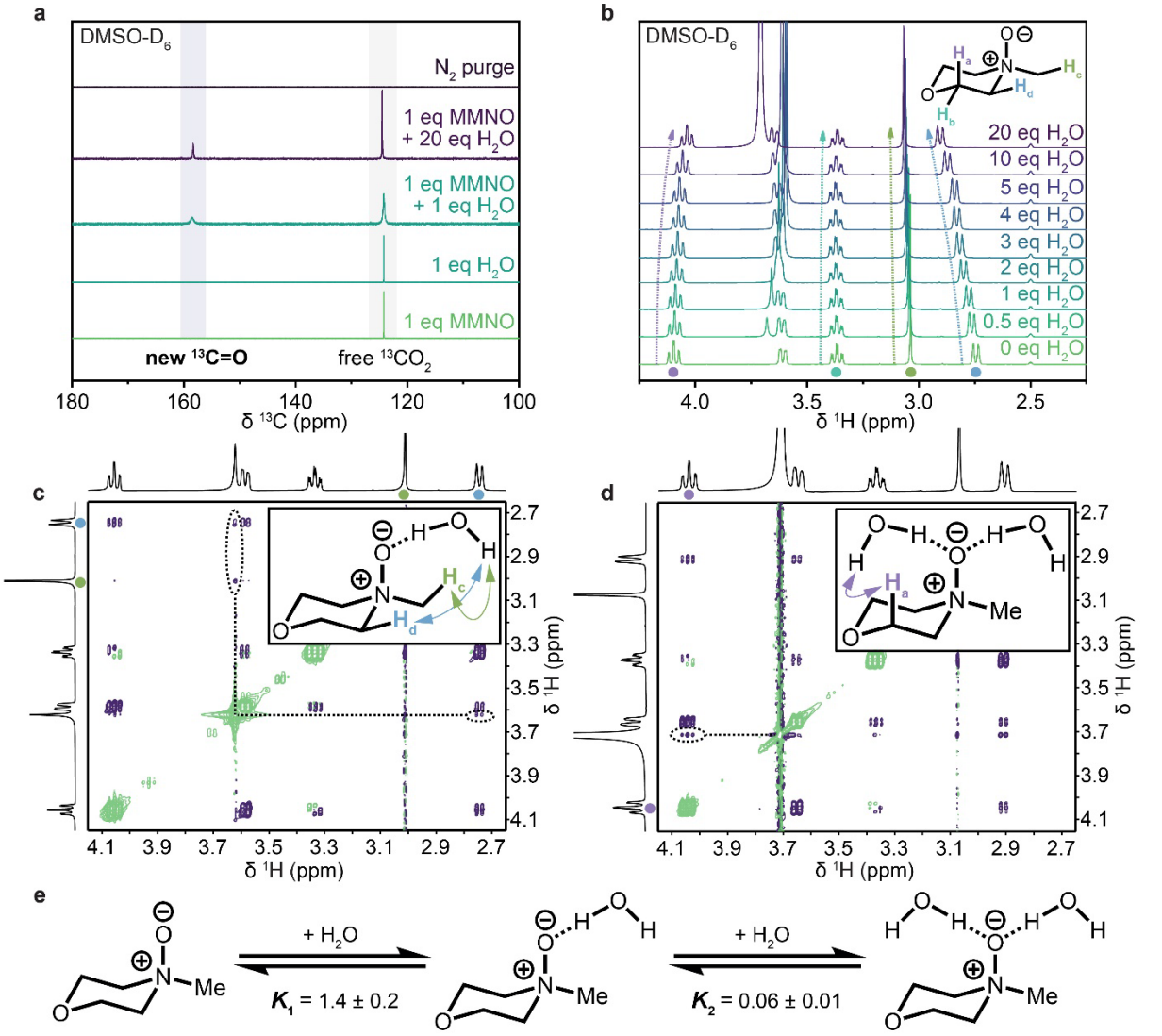

Fig. 2. Role of water in MMNO-H_2O-DMSO system | a, $^{13}C\{^1H\}$ NMR spectra of $^{13}CO_2$-dosed MMNO (0.25 M, DMSO-D_6) with different equivalents of water, control experiments with no MMNO, and after N_2 purging for 1 hour. **b**, ^1H NMR spectra of NMR titration experiments of MMNO (host, 0.25 M in DMSO-D_6) and water (guest, 0, 0.5, 1, 2, 3, 4, 5, 10, 20 equivalents). H_a, H_b, H_c, H_d for MMNO were tracked for perturbation. See Supplementary Information for experiments with other host concentrations. **c**, 2D NOESY spectrum of MMNO (0.25 M, DMSO-D_6) with 1 equivalent of water at 25 °C at a mixing time of 600 ms. **d**, 2D NOESY spectrum of MMNO (0.25 M, DMSO-D_6) with 20 equivalents of water at 25 °C at a mixing time of 600 ms. **e**, The most plausible mechanism (1:2 full model) of MMNO-H_2O host-guest binding determined from the NMR titration experiments via NMR data fitting using nonlinear regression methods, and association constants (K_1 and K_2). See Supplementary Information for details of theories and calculations. Numbers are reported as "average ± standard error" among three experiments with different host concentrations.

Mechanism of CO_2 capture with MMNO•H_2O

To interrogate the formation of MMNO•H_2O•$^{13}CO_2$, NMR titration experiments with MMNO (0.25 M in DMSO-D_6) in the presence of $^{13}CO_2$ were conducted (Fig. 3a). By integrating the resonances corresponding to dissolved $^{13}CO_2$ and MMNO•H_2O•$^{13}CO_2$, the relative mole fractions of both species as a function of H_2O equivalents added could be determined (Fig. 3b). The mole fraction of MMNO•H_2O•$^{13}CO_2$ relative to dissolved $^{13}CO_2$ maximizes at 2–10 equivalents of H_2O added relative to MMNO, which is a similar MMNO:H_2O ratio at which the concentration of MMNO•H_2O maximizes in the absence of CO_2 (highlighted with green in Fig. 3b). This finding indicates that MMNO•H_2O is likely responsible for CO_2 capture under these conditions. Likewise, dosing $^{13}CO_2$ into solutions of MMNO in D_2O (spanning from ~22 to ~222 equivalents of D_2O) yields a new resonance (~160 ppm) corresponding to a MMNO•$^{13}CO_2$ adduct, which was not observed in D_2O alone (Fig. 3c). Furthermore, the relative integrations of free $^{13}CO_2$ and this adduct showed a negative correlation between the concentration of MMNO•$^{13}CO_2$ and the D_2O:MMNO ratio.

Although observing MMNO•H_2O•$^{13}CO_2$ directly by ^{1}H NMR is challenging due to the dynamic fast-exchange nature of $^{13}CO_2$ binding on the ^{1}H NMR time scale (Supplementary Fig. 14), the chemical shift observed for H_2O further supports the formation of a $^{13}CO_2$ adduct. For example, at 4 equivalents of H_2O relative to MMNO in DMSO-D_6 (see Supplementary Figs. 14–17 for other equivalents), the exchange among free H_2O, H_2O•MMNO, and MMNO•$(H_2O)_2$ results in a shift downfield from 3.4 ppm to 3.6 ppm due to strong hydrogen-bonding interactions between H_2O and MMNO (Fig. 3d). Markedly, in the presence of $^{13}CO_2$, the resonance of H_2O shifts to 3.9 ppm and further broadens (Fig. 3d), which likely results from exchanging with a new species possessing a much more downfield-shifted proton (i.e., MMNO•H_2O•$^{13}CO_2$) on top of the exchange pathways discussed above.

Based on the observations above, the most likely mechanistic scenario is that MMNO•H_2O—and not free MMNO—reacts with CO_2 via carbonic acid (H_2CO_3, p$K_{a(apparent)}$ ~6)[43,44], HCO_3^- (pK_a ~10)[43], or CO_3^{2-} formation. The latter is unfavored because, unlike amines, MMNO is not basic enough to deprotonate HCO_3^- to form CO_3^{2-}. An alternative mechanistic pathway in which the oxygen of the *N*-oxide directly attacks CO_2 was ruled out based on ^{15}N and ^{1}H–^{13}C 2D HMBC spectroscopies and density functional theory (DFT) calculations (see Supplementary Figs. 42, 43, and DFT discussions). To distinguish among these possibilities, ^{13}C NMR experiments were conducted to benchmark the chemical shift of the CO_2 adduct formed with MMNO•H_2O in D_2O against various HCO_3^- and CO_3^{2-} salts (Fig. 3e). The experimental ^{13}C NMR chemical shift of MMNO•$^{13}CO_2$ in D_2O (160 ppm) is closer to that observed for HCO_3^- (160.6–160.7 ppm) than for CO_3^{2-} (161.1–168.5 ppm) or that predicted for H_2CO_3 (152 ppm, see Supplementary Table 4 for computational details). Furthermore, the pH was monitored when CO_2 was bubbled through a 0.25 M aqueous MMNO solution and ultrapure water for comparison (Fig. 3f and Supplementary Fig. 41). In pure water, the pH drops and then stabilizes at 4.36, at which only dissolved CO_2 and H_2CO_3 are present[43,45]. However, in the presence of MMNO, a steady state at pH 6.19 was observed,

corresponding to the apparent pK_1 of 6.35 at which no CO_3^{2-} is present in aqueous solutions[43]. Together, these findings support that carbon capture with MMNO•H_2O occurs via formation of a HCO_3^- species stabilized by hydrogen bonding with MMNO.

DFT calculations were next performed with Gaussian 16[46] at the ωB97XD[47] level of theory at 298.15 K in DMSO as the solvent to support the proposed pathway (Fig. 3g). Optimized structures of MMNO•H_2O(**A**) and MMNO•$(H_2O)_2$ were found to have H_2O bound in preferred orientations that match well with the NOESY experiments (Fig. 3g and Fig. 2c–d; see Supplementary Information for the less favored MMNO•H_2O(**B**)). Three possible and energetically similar adducts (**1**–**3**) based on different conformations[48–51] of MMNO–$H^+\cdots HCO_3^-$ or MMNO$\cdots H_2CO_3$ can be envisioned (Fig. 3g). For structures **2** and **3**, the O$\cdots$O distances (2.45 Å for **2**, 2.44 Å for **3**) for the most important hydrogen bond interactions (O–$H^+\cdots O^-$) are much shorter than in **1** (2.55 Å and 2.58 Å), within the range of strong hydrogen-bonding interactions (2.2–2.5 Å)[52]. Further, C–H$\cdots$O interactions are also predicted in optimized structures **2** and **3**. The ^{13}C chemical shifts corresponding to the C=O carbons in **1**–**3** were also predicted using the gauge-independent atomic orbitals method[53,54] at the same level of theory in DMSO (see Supplementary Table 4 for chemical shift calculations in H_2O). The calculated chemical shift (155 ppm) of **3** agrees best with the experimental chemical shift (159 ppm) of MMNO•H_2O•$^{13}CO_2$ in DMSO-D_6, making **3** the most plausible structure for this adduct. However, due to the highly dynamic nature of this reaction, we cannot rule out involvement of other species. Further, our calculations also support that MMNO•H_2O reacting with CO_2 is favored by $\Delta\Delta H$ = 2.34–2.98 kcal/mol compared to MMNO•$(H_2O)_2$ formation, supporting that CO_2 capture is still favored even in the presence of excess H_2O. The calculated CO_2 binding enthalpy for **3** relative to MMNO•H_2O is only −9.53 kcal/mol, which is significantly less downhill than that normally observed for amines (<−12 kcal/mol)[16]. This finding explains why MMNO•H_2O•CO_2 can release CO_2 easily (~65 °C under pure CO_2 atmosphere), whereas most amines must be heated above 100 °C to be regenerated in a temperature swing process.

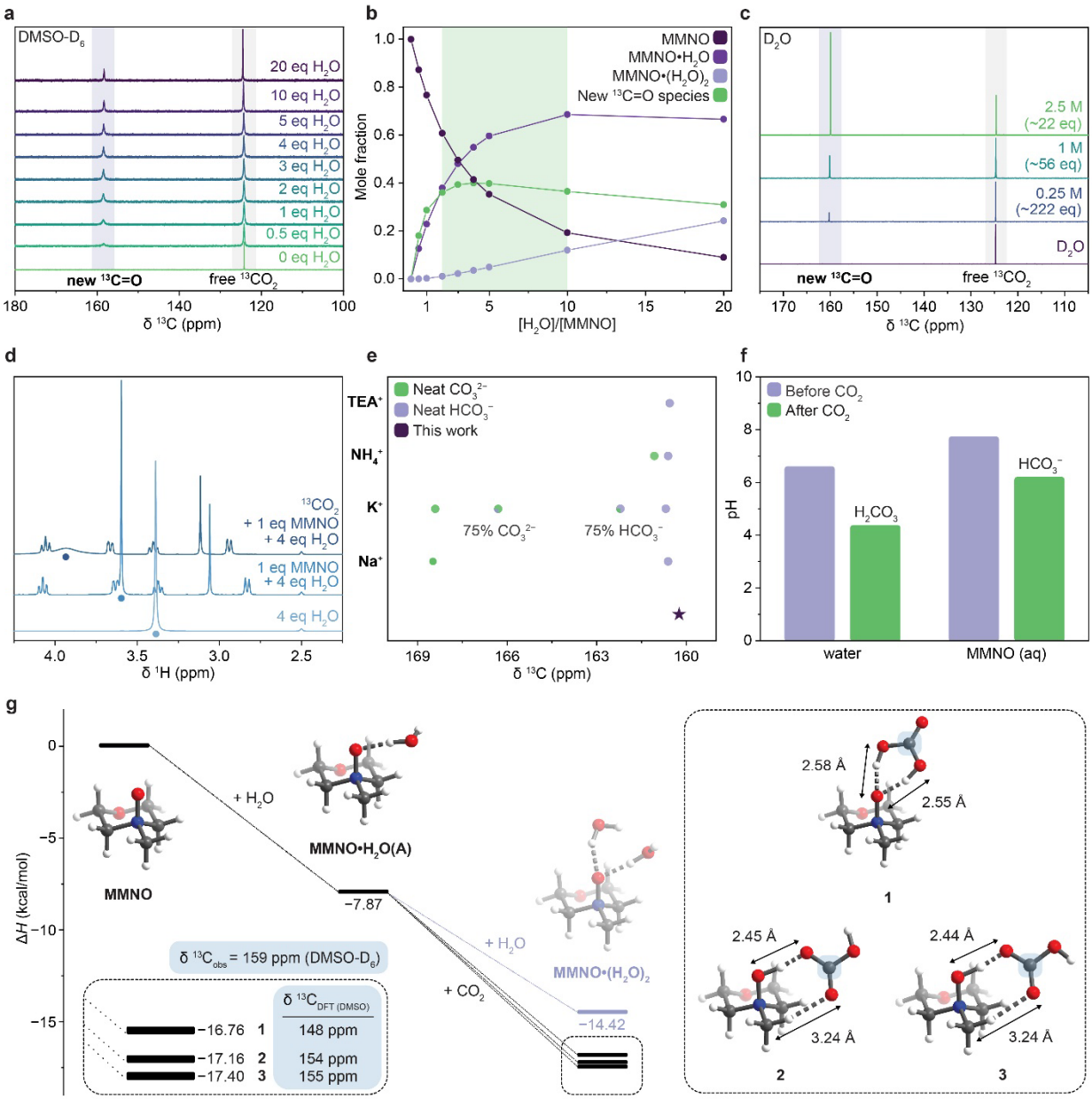

Fig. 3. Mechanism investigation and product identification | a, $^{13}C\{^1H\}$ spectrum of MMNO (0.25 M, DMSO-D_6) dosed with $^{13}CO_2$ with different equivalents of water. **b**, Mole fractions of new ^{13}C=O species (versus total ^{13}C species) from the integrations and mole fractions of free MMNO, MMNO•H_2O, and MMNO•$(H_2O)_2$ (versus total MMNO species) from the output parameters of the NMR titration data fitting. **c**, $^{13}C\{^1H\}$ spectrum of MMNO (D_2O) dosed with $^{13}CO_2$ with different concentrations, and corresponding equivalents of water. **d**, ^1H NMR spectrum of 4 equivalents of water (DMSO-D_6) without and with 1 equivalent of MMNO (0.25 M), and with both MMNO and $^{13}CO_2$. See supplementary materials for other equivalents of water. **e**, A comparison of the ^{13}C NMR chemical shift in D_2O for the product detected in this study with other common (bi)carbonate compounds in D_2O. Observed ^{13}C chemical shifts for K^+ mixtures ("75% HCO_3^-" and "75% CO_3^{2-}") only showed a single chemical shifts due to the fast exchange of the proton between $KHCO_3$ and K_2CO_3[55]. **f**, pH before and after pure water and 0.25 M aqueous MMNO solution were equilibrated with CO_2 bubbling for 11 min at room temperature (21–22 °C). **g**, DFT-calculated enthalpy changes and optimized geometries of MMNO and its hydrates, along with three different proposed structures for the product

https://doi.org/10.26434/chemrxiv-2024-817j5 **ORCID:** https://orcid.org/0000-0002-2618-013X

(**1**, **2**, and **3**). Calculated ^{13}C NMR chemical shifts for C=O carbons in **1**–**3** compared to the observed chemical shift (both in DMSO(-D_6) as the solvent). See Methods and Supplementary Information for DFT methods.

Carbon capture cyclability, performance, and stability

The studies outlined above support that MMNO•H_2O can reversibly react with CO_2 to form MMNO–$H^+\cdots HCO_3^-$ (**3**), representing a new pathway for CO_2 absorption. To validate that this mechanism enables carbon capture under realistic conditions, the cyclability of CO_2 binding were evaluated using infrared (IR) spectroscopy. Owing to its reasonable saturation time and ease of preparation, a 1:4 (v:v) mixture of commercially available 50 wt. % (~6.5 equivalents of water) aqueous MMNO solution and DMSO was employed for these measurements (both components used directly as received). Upon bubbling CO_2 (6 sccm, see Supplementary Note 2), two new characteristic C=O stretches at 1656 cm^{-1} and 1716 cm^{-1} were found to increase in intensity over time (Fig. 4a), which can be attributed to the formation of MMNO–$H^+\cdots HCO_3^-$. Indeed, DFT-calculated vibrational frequencies of proposed products **2** and **3** reveal a similar two-peak profile in the range of 1550–1800 cm^{-1} (see Supplementary Figs. 47–48 and Supplementary Note 4). Upon purging the solution with N_2, these signals disappear, consistent with the reversibility of CO_2 binding observed by ^{13}C NMR (Fig. 2a). Emulating a vacuum-swing process, pure CO_2 was bubbled through the MMNO solution (6 sccm) for 1 hour, followed by pure N_2 (6 sccm) for 1 hour. Good reversibility was observed over seven cycles, with the last four cycles showing nearly identical profiles (Fig. 4b, see Supplementary Fig. 23 for the first three cycles before stabilizing). Absorption and desorption were largely completed in less than 30 minutes; in addition, viscosity measurements revealed that this solution retained low viscosities both before and after CO_2 dosing (Supplementary Fig. 40). Gravimetric CO_2 capacities were also measured by weighing solutions before and after 1 hour of absorption, corrected by solvent controls under the same conditions (see Supplementary Information for details, Supplementary Table 2, 3 for data). We determined that the MMNO solution reaches a capacity of 2.32 mmol CO_2/g MMNO under a pure CO_2 stream in 1 hour (Fig. 4c).

To evaluate whether MMNO•H_2O can remove CO_2 from dilute, mixed gas streams, 50% and 15% CO_2 mixtures in N_2 were flowed through the same MMNO solution (Fig. 4c). Good capacities (1.48 and 0.92 mmol CO_2/g MMNO, respectively) were still observed by IR and gravimetric measurements after 1 hour under these conditions. However, real flue gas streams contain contaminants other than N_2, including O_2, H_2O, NO_x, and SO_x, that can lead to sorbent degradation[3]. A sample of flue gas from the Cornell Combined Heat and Power (CHP) natural gas-fired power plant—consisting of 9.7% CO_2, 3.8% O_2, 43 ppm NO_x, remainder H_2O and N_2—was obtained to test the CO_2 capture capability of MMNO•H_2O from an industrial waste stream. Remarkably, we determined that MMNO•H_2O can capture CO_2 from this flue gas to reach a capacity of 0.70 mmol CO_2/g MMNO after 1 hour, with no additional stretches observed due to sorbent degradation by IR (Supplementary Fig. 28).

One of the major limitations of amine-based scrubbers is their poor long-term cycling stability arising from oxidative and thermal degradation[3,19]. Indeed, heating the amines 4-methyl

morpholine (MM) and 1-methylpiperazine (MP), two close structural analogs of MMNO, and monoethanolamine (MEA), a benchmark amine for carbon capture, in D_2O for 1 week at 100 °C under flue gas led to the formation of insoluble impurities (Fig. 5d). More degradation was observed for MM, MP, and MEA in wet DMSO-D_6 after the same accelerated aging studies: the solutions became darkly colored, and numerous new species were observed by ^{1}H NMR (Supplementary Figs. 36–38). In contrast, MMNO exhibits excellent stability after being heated in both D_2O and wet DMSO-D_6 at 100 °C under flue gas (Fig. 5d). No degradation was observed in D_2O (Supplementary Fig. 34), and the only degradation product observed upon extended heating in DMSO-D_6 under flue gas was MM, likely due to slow O atom transfer from MMNO to the solvent (Supplementary Fig. 35). Notably, MM can be easily reoxidized to MMNO with hydrogen peroxide in the presence of CO_2 as the catalyst[26,56], offering a potential method for sorbent regeneration after extended cycling.

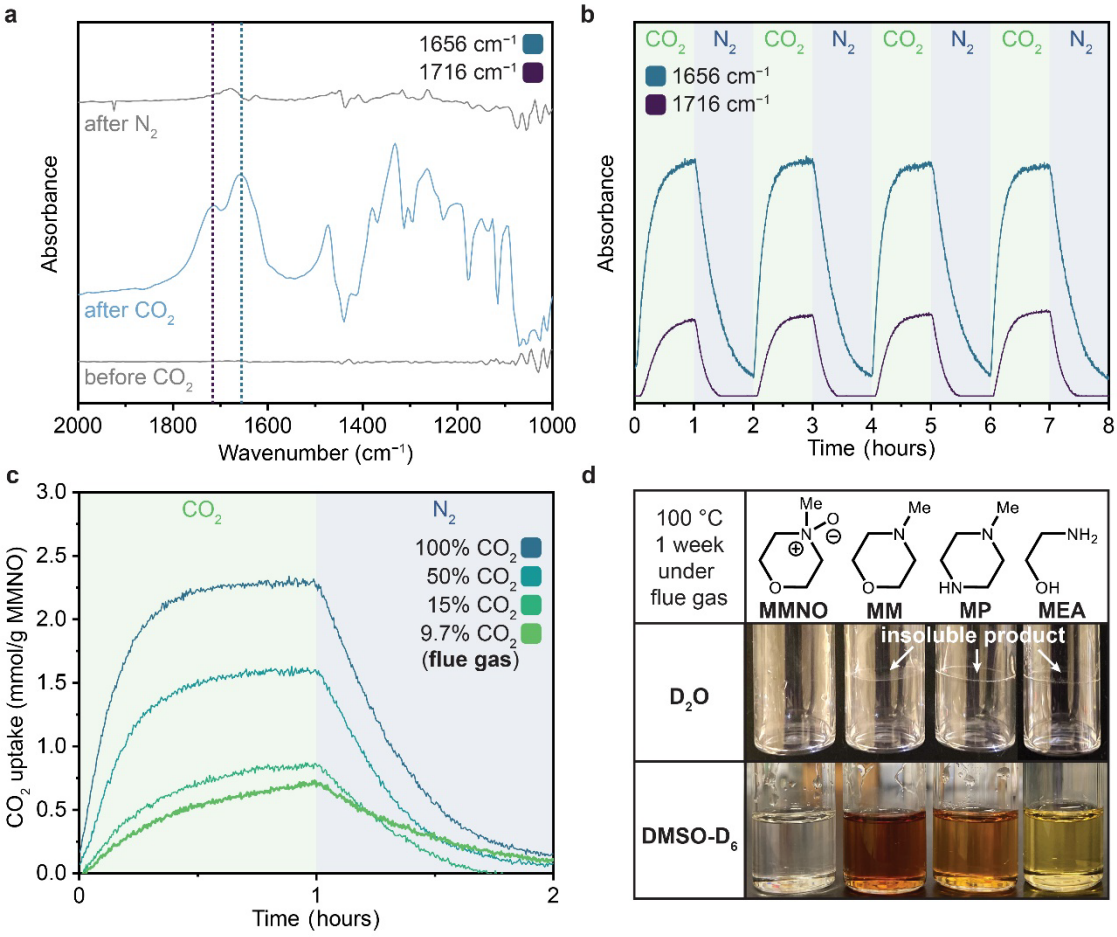

Fig. 4. CO_2 cyclability and MMNO stability | a, The *in situ* IR spectrum of 1:4 (v:v) 50 wt. % MMNO(aq): DMSO before CO_2 bubbling, after CO_2 (100%) bubbling (absorption) and after N_2 bubbling (desorption). Stretches at 1716 and 1656 cm^{-1} are assigned to the product(s). **b**, IR trend tracking for stretches 1716 and 1656 cm^{-1} of CO_2 (100%) absorption-desorption cycles 4–7 at 6 sccm using 1:4 (v:v) 50 wt. % MMNO(aq): DMSO at room temperature (21–22 °C). **c**, The CO_2 capacity trend of one CO_2 absorption-desorption cycle with 1:4 (v:v) 50 wt. % MMNO(aq):DMSO

using 100%, 50%, 15% CO_2 in N_2 mixtures, and flue gas from Cornell University's natural gas-fired power plant (9.7% CO_2) at 6 sccm at room temperature (21–22 °C). **d**, Appearances after accelerated aging studies for MMNO, 4-methylmorpholine (MM), 1-methylpiperazine (MP), and monoethanolamine (MEA) with heating at 100 °C for 1 week in D_2O or DMSO-D_6 under flue gas.

Conclusion

Given the immediacy of the looming climate crisis, we urgently need new sorbents that can be rapidly scaled and employed in engineering configurations that have already been optimized for amine-based scrubbers. The presented gas sorption, spectroscopic, and computational studies support that the monohydrates of tertiary amine *N*-oxides, one of the oxidative byproducts arising from CO_2 capture with tertiary amines[6,7], can capture CO_2 via a new hydrogen-bonding pathway. The inexpensive MMNO is robust towards oxygen and high temperatures while exhibiting good CO_2 uptake from dilute streams, including flue gas from a natural gas-fired power plant. Given the relatively low heat of absorption of this system, it could also offer opportunities for high-feed-pressure systems. Our findings lay the groundwork for the further development of small-molecule and polymeric tertiary amine *N*-oxides as non-basic sorbents for challenging CO_2 separations.

Methods

$^{13}CO_2$ dosing with controlled water amount

In a N_2-filled glovebox, MMNO (dried by vacuum sublimation) and DMSO-D_6 (dried over molecular sieves) were added to a screw-cap NMR tube (dried at 165 °C for 12 hours). The tube was then sealed and brought out of glovebox. Alternatively, D_2O (instead of DMSO-D_6) or DI water was added quickly outside the glovebox. Subsequently, the sample was dosed with $^{13}CO_2$ (99 atom % ^{13}C, <3 atom % ^{18}O) on the custom-built setup after degassing (cooling to −78 °C for DMSO-D_6 or 0 °C for D_2O).

NMR Chemical Shift Perturbation Titration

DI water (1, 2, 4, 6, 8, 10, 20, 40 equiv. for 0.125 M; 0.5, 1, 1.5, 2, 2.5, 5, 10, 20 equiv. for 0.2 M; 0.25, 0.5, 1, 1.5, 2, 2.5, 5, 10 equiv. for 0.5 M) was added quickly to the NMR tube with ($^{13}CO_2$ dosed) MMNO solutions in DMSO-D_6. The mixture obtained at each titration point was shaken thoroughly for 1 min and allowed to equilibrate in the NMR probe for 5 min before the spectra were recorded. All NMR spectra were recorded at 25 °C. The data were fitted to the built-in mathematical models in Bindfit[40].

NMR spectroscopy

^1H, ^{13}C, ^1H–^1H NOESY, ^1H–^{15}N HMBC NMR spectra were all recorded on Bruker or Varian 500 MHz spectrometers, ^1H–^{13}C HMBC was recorded on a Varian 600 MHz spectrometer. In the cases of DMSO-D_6, spectra were referenced to 2.50 ppm for ^1H NMR and 39.52 ppm for ^{13}C NMR. In the cases of D_2O, spectra were referenced to 4.79 ppm for ^1H NMR, and 77.16 ppm (for $CDCl_3$ inserts) or using the absolute reference function in Mestrenova for ^{13}C NMR.

IR measurements

Infrared spectra were recorded with ReactIR™ iC10 FTIR spectrometer fitted with a 30-bounce, silicon-tipped probe. 100%, 50%, and 15% CO_2 (in N_2), flue gas (from Cornell Combined Heat and Power Plant, 9.7% CO_2, 3.8% O_2, 43 ppm NO_x, remainder H_2O and N_2), and 100% N_2 were dosed through the custom-built setups at 6 sccm or 6 mL/min. During a regular carbon capture cycle, CO_2-containing streams were bubbled through a 5 mL 1:4 (v:v) 50 wt. % MMNO(aq):DMSO solution (used as received) for 1 hour, then the streams were switched to 100% N_2 for 1 hour to simulate vacuum swing processes for desorption. The cycling experiments were all done at room temperature (21–22 °C).

Gravimetric measurements

Empty vials with septa caps were tared, and then 50 wt. % MMNO (aq) and DMSO (used as received) were added to make total of 5 mL solutions. For control experiments, the same amounts of DI water and DMSO were added instead. The total masses were recorded, and then a 100%, 50% or 15% CO_2 in N_2 mixture was bubbled through the mixtures for 1 hour. After bubbling, the masses were recorded again. All experiments were conducted in triplicate. The measurements were done at room temperature (21–22 °C).

Viscosity measurements

Viscosities of 22 mL 1:4 (v:v) 50 wt. % MMNO(aq):DMSO solution before and after 100% CO_2 dosing (1.5 h, room temperature) were measured on Discovery Hybrid Rheometer HR-3 (TA Instruments) equipped with Peltier Concentric Cylinder system using a geometry of DIN conical rotor and standard cup. Viscosities were measured at a shear rate of 300 s^{-1} at 25, 45, 65, and 85 °C.

pH measurements

pH measurements were conducted with a HI 221 Calibration Check Microprocessor pH Meter. A 3-point calibration (with pH 4, pH 7, and pH 10 buffers) was performed before the measurement. Measurements were performed on both ultrapure water and 0.25 M MMNO in DI water (both 6 mL). pH readings on the pH meter were recorded every 10 s.

DFT calculations

All DFT calculations were performed using Gaussian 16 package[46] at the ωB97XD[47] level of theory at 298.15 K. A pruned (99, 590) integration grid (equivalent to Gaussian's "UltraFine" option) was used for all calculations. The self-consistent reaction field (SCRF) was used to model systems in DMSO as the solvent by using SMD (solvation model density) solvation model[57]. All geometries were optimized with the def2-SVP basis set[58,59]. A vibrational frequency analysis was conducted at the same level of theory as the geometry optimizations (ωB97XD/def2-SVP). The optimized geometries characterized as local minima on the potential energy surfaces (PES) have no imaginary frequencies. For improved accuracy single point energies were calculated with the same dispersion corrected ωB97XD functional using the slightly larger (def2-TZVP) basis set[58,59] of the same family. ^{13}C NMR chemical shifts of C=O carbons in structures **1**, **2**, and **3** in both water and DMSO were predicted by using DFT at their optimized geometries by employing GIAO (gauge-independent atomic orbitals) method[53,54], with tetramethylsilane (TMS) as the reference (0 ppm) calculated at the same level of theory. The isotropic magnetic shielding tensors were averaged over all symmetric carbons when applicable.

References

1. International Energy Agency (IEA). *The Role of CCUS in Low-Carbon Power Systems*. https://www.iea.org/reports/the-role-of-ccus-in-low-carbon-power-systems (2020).
2. Rochelle, G. T. Amine Scrubbing for CO_2 Capture. *Science* **325**, 1652–1654 (2009).
3. Gouedard, C., Picq, D., Launay, F. & Carrette, P.-L. Amine degradation in CO_2 capture. I. A review. *Int. J. Greenh. Gas Control* **10**, 244–270 (2012).
4. McDonald, J. D. *et al.* Carbon Capture and Sequestration: An Exploratory Inhalation Toxicity Assessment of Amine-Trapping Solvents and Their Degradation Products. *Environ. Sci. Technol.* **48**, 10821–10828 (2014).
5. Mazari, S. A. *et al.* Review of modelling and simulation strategies for evaluating corrosive behavior of aqueous amine systems for CO_2 capture. *Int. J. Greenh. Gas Control* **96**, 103010 (2020).
6. Lepaumier, H. Study of the degradation mechanisms of amines used for the capture of CO_2 in industrial fumes. (Universite de Savoie, Le Bourget-du-Lac, France, 2008).
7. Voice, A. K. Amine oxidation in carbon dioxide capture by aqueous scrubbing. (The University of Texas at Austin, Austin, TX, 2013).
8. United Nations Framework Convention on Climate Change (UNFCCC). The Paris Agreement. (2015).
9. Amici, A., Barghini, A., Cucchi, M., Correa-Mendes, M., Buontempo, C., Vamborg, F. & Simmons, A. How close are we to reaching a global warming of 1.5°C? Copernicus Climate Change Service (2021) https://cds.climate.copernicus.eu/cdsapp#!/software/app-c3s-global-temperature-trend-monitor?tab=app.
10. International Energy Agency (IEA), Capacity of current and planned large-scale CO_2 capture projects vs. the Net Zero Scenario, 2020–2030 (2023); https://www.iea.org/data-and-statistics/charts/capacity-of-current-and-planned-large-scale-co2-capture-projects-vs-the-net-zero-scenario-2020-2030.
11. Global CCS Institute. *Global Status of CCS 2024: Collaborating for a Net-Zero Future*. https://www.globalccsinstitute.com/resources/global-status-report/ (2024).
12. Lyons, M., Durrant, P. & Kochhar, K. *Reaching Zero with Renewables: Capturing Carbon*. https://www.irena.org/Technical-Papers/Capturing-Carbon (2021).
13. Cozzi, L. *et al. Net Zero by 2050: A Roadmap for the Global Energy Sector*. https://www.iea.org/reports/net-zero-by-2050 (2021).
14. Bottoms, R. R. Separating acid gases. U.S. Patent 1783901 (1930).

15. Rochelle, G. T., Bishnoi, S., Chi, S., Dang, H. & Santos, J. Research needs for CO_2 capture from flue gas by aqueous absorption/stripping, Final report for P.O. No. DE-AF26-99FT01029. (2001).
16. Xu, Q. Thermodynamics of CO_2 loaded aqueous amines. (The University of Texas at Austin, Austin, TX, 2011).
17. Aaron, D. & Tsouris, C. Separation of CO_2 from Flue Gas: A Review. *Sep. Sci. Technol.* **40**, 321–348 (2005).
18. Meng, F. *et al.* Research progress of aqueous amine solution for CO_2 capture: A review. *Renew. Sustain. Energy Rev.* **168**, 112902 (2022).
19. Rochelle, G. T. Thermal degradation of amines for CO_2 capture. *Curr. Opin. Chem. Eng.* **1**, 183–190 (2012).
20. Dumée, L., Scholes, C., Stevens, G. & Kentish, S. Purification of aqueous amine solvents used in post combustion CO_2 capture: A review. *Int. J. Greenh. Gas Control* **10**, 443–455 (2012).
21. Wang, T., Hovland, J. & Jens, K. J. Amine reclaiming technologies in post-combustion carbon dioxide capture. *J. Environ. Sci.* **27**, 276–289 (2015).
22. Vevelstad, S. J., Buvik, V., Knuutila, H. K., Grimstvedt, A. & Da Silva, E. F. Important Aspects Regarding the Chemical Stability of Aqueous Amine Solvents for CO_2 Capture. *Ind. Eng. Chem. Res.* acs.iecr.2c02344 (2022) doi:10.1021/acs.iecr.2c02344.
23. Rao, A. B. & Rubin, E. S. A Technical, Economic, and Environmental Assessment of Amine-Based CO_2 Capture Technology for Power Plant Greenhouse Gas Control. *Environ. Sci. Technol.* **36**, 4467–4475 (2002).
24. Veltman, K., Singh, B. & Hertwich, E. G. Human and Environmental Impact Assessment of Postcombustion CO_2 Capture Focusing on Emissions from Amine-Based Scrubbing Solvents to Air. *Environ. Sci. Technol.* **44**, 1496–1502 (2010).
25. Rochelle, G. T. Air pollution impacts of amine scrubbing for CO_2 capture. *Carbon Capture Sci. Technol.* **11**, 100192 (2024).
26. Kobus, M., Friedrich, T., Zorn, E., Burmeister, N. & Maison, W. Medicinal Chemistry of Drugs with *N*-Oxide Functionalities. *J. Med. Chem.* **67**, 5168–5184 (2024).
27. Singh, S. K., Bajpai, M. & Tyagi, V. K. Amine Oxides: A Review. *J. Oleo Sci.* **55**, 99–119 (2006).
28. Clewell, R. A. *et al.* An in vitro approach to determine the human relevance of anti-spermatogenic effects of 4-methylmorpholine 4-oxide, monohydrate (NMMO) in rat reproductive toxicity studies. *Toxicol. In Vitro* **82**, 105365 (2022).

29. Yancey, P. H., Blake, W. R. & Conley, J. Unusual organic osmolytes in deep-sea animals: adaptations to hydrostatic pressure and other perturbants. *Comp. Biochem. Physiol. A. Mol. Integr. Physiol.* **133**, 667–676 (2002).

30. Yancey, P. H. Organic osmolytes as compatible, metabolic and counteracting cytoprotectants in high osmolarity and other stresses. *J. Exp. Biol.* **208**, 2819–2830 (2005).

31. Fink, H.-P., Weigel, P., Purz, H. J. & Ganster, J. Structure formation of regenerated cellulose materials from NMMO-solutions. *Prog. Polym. Sci.* **26**, 1473–1524 (2001).

32. Perepelkin, K. E. Lyocell fibres based on direct dissolution of cellulose in N-methylmorpholine N-oxide: Development and prospects. *Fibre Chem.* **39**, 163–172 (2007).

33. Acharya, S. *et al.* Utilization of Cellulose to Its Full Potential: A Review on Cellulose Dissolution, Regeneration, and Applications. *Polymers* **13**, 4344 (2021).

34. Qiao, H., Li, M., Wang, C., Zhang, Y. & Zhou, H. Progress, Challenge, and Perspective of Fabricating Cellulose. *Macromol. Rapid Commun.* **43**, 2200208 (2022).

35. Li, B. *et al.* Trimethylamine *N*-oxide–derived zwitterionic polymers: A new class of ultralow fouling bioinspired materials. *Sci. Adv.* **5**, eaaw9562 (2019).

36. Scholten, H. & Rindtorff, K. Process for producing aqueous N-methylmorpholine-N-oxide solutions.

37. Chanzy, H., Nawrot, S., Peguy, A., Smith, P. & Chevalier, J. Phase behavior of the quasiternary system *N*-methylmorpholine-*N*-oxide, water, and cellulose. *J. Polym. Sci. Polym. Phys. Ed.* **20**, 1909–1924 (1982).

38. Claridge, T. D. W. Dynamic Effects in NMR. in *High-Resolution NMR Techniques in Organic Chemistry* 38–57 (Elsevier, 2016). doi:10.1016/B978-0-08-099986-9.00001-4.

39. Pike, S. J., Hutchinson, J. J. & Hunter, C. A. H-Bond Acceptor Parameters for Anions. *J. Am. Chem. Soc.* **139**, 6700–6706 (2017).

40. Thordarson, P. BindFit. http://app.supramolecular.org/bindfit/.

41. Thordarson, P. Determining association constants from titration experiments in supramolecular chemistry. *Chem Soc Rev* **40**, 1305–1323 (2011).

42. Brynn Hibbert, D. & Thordarson, P. The death of the Job plot, transparency, open science and online tools, uncertainty estimation methods and other developments in supramolecular chemistry data analysis. *Chem. Commun.* **52**, 12792–12805 (2016).

43. Pedersen, O., Colmer, T. D. & Sand-Jensen, K. Underwater Photosynthesis of Submerged Plants – Recent Advances and Methods. *Front. Plant Sci.* **4**, (2013).

44. Pines, D. *et al.* How Acidic Is Carbonic Acid? *J. Phys. Chem. B* **120**, 2440–2451 (2016).

45. Zhong, H., Fujii, K., Nakano, Y. & Jin, F. Effect of CO_2 Bubbling into Aqueous Solutions Used for Electrochemical Reduction of CO_2 for Energy Conversion and Storage. *J. Phys. Chem. C* **119**, 55–61 (2015).

46. Frisch, M. J.; Trucks, G. W.; Schlegel, H. B.; Scuseria, G. E.; Robb, M. A.; Cheeseman, J. R.; Scalmani, G.; Barone, V.; Petersson, G. A.; Nakatsuji, H.; Li, X.; Caricato, M.; Marenich, A. V.; Bloino, J.; Janesko, B. G.; Gomperts, R.; Mennucci, B.; Hratchian, H. P.; Ortiz, J. V.; Izmaylov, A. F.; Sonnenberg, J. L.; Williams-Young, D.; Ding, F.; Lipparini, F.; Egidi, F.; Goings, J.; Peng, B.; Petrone, A.; Henderson, T.; Ranasinghe, D.; Zakrzewski, V. G.; Gao, J.; Rega, N.; Zheng, G.; Liang, W.; Hada, M.; Ehara, M.; Toyota, K.; Fukuda, R.; Hasegawa, J.; Ishida, M.; Nakajima, T.; Honda, Y.; Kitao, O.; Nakai, H.; Vreven, T.; Throssell, K.; Montgomery, J. A., Jr.; Peralta, J. E.; Ogliaro, F.; Bearpark, M. J.; Heyd, J. J.; Brothers, E. N.; Kudin, K. N.; Staroverov, V. N.; Keith, T. A.; Kobayashi, R.; Normand, J.; Raghavachari, K.; Rendell, A. P.; Burant, J. C.; Iyengar, S. S.; Tomasi, J.; Cossi, M.; Millam, J. M.; Klene, M.; Adamo, C.; Cammi, R.; Ochterski, J. W.; Martin, R. L.; Morokuma, K.; Farkas, O.; Foresman, J. B.; Fox, D. J. Gaussian 16, Revision C.01; Gaussian, Inc., Wallingford CT, 2016.

47. Chai, J.-D. & Head-Gordon, M. Long-range corrected hybrid density functionals with damped atom–atom dispersion corrections. *Phys. Chem. Chem. Phys.* **10**, 6615 (2008).

48. Jönsson, B., Karlström, G., Wennerström, H. & Roos, B. Ab initio molecular orbital calculations on the water-carbon dioxide system: carbonic acid. *Chem. Phys. Lett.* **41**, 317–320 (1976).

49. Nguyen Minh Tho & Ha, T. K. A theoretical study of the formation of carbonic acid from the hydration of carbon dioxide: a case of active solvent catalysis. *J. Am. Chem. Soc.* **106**, 599–602 (1984).

50. Mori, T., Suma, K., Sumiyoshi, Y. & Endo, Y. Spectroscopic detection of isolated carbonic acid. *J. Chem. Phys.* **130**, 204308 (2009).

51. Reddy, S. K. & Balasubramanian, S. Carbonic acid: molecule, crystal and aqueous solution. *Chem Commun* **50**, 503–514 (2014).

52. Nygren, C. L., Wilson, C. C. & Turner, J. F. C. Electron and Nuclear Positions in the Short Hydrogen Bond in Urotropine-*N*-oxide·Formic Acid. *J. Phys. Chem. A* **109**, 1911–1919 (2005).

53. Wolinski, K., Hinton, J. F. & Pulay, P. Efficient implementation of the gauge-independent atomic orbital method for NMR chemical shift calculations. *J. Am. Chem. Soc.* **112**, 8251–8260 (1990).

54. Cheeseman, J. R., Trucks, G. W., Keith, T. A. & Frisch, M. J. A comparison of models for calculating nuclear magnetic resonance shielding tensors. *J. Chem. Phys.* **104**, 5497–5509 (1996).

55. Mani, F., Peruzzini, M. & Stoppioni, P. CO_2 absorption by aqueous NH_3 solutions: speciation of ammonium carbamate, bicarbonate and carbonate by a ^{13}C NMR study. *Green Chem.* **8**, 995 (2006).

56. Balagam, B. & Richardson, D. E. The Mechanism of Carbon Dioxide Catalysis in the Hydrogen Peroxide N-Oxidation of Amines. *Inorg. Chem.* **47**, 1173–1178 (2008).

57. Marenich, A. V., Cramer, C. J. & Truhlar, D. G. Universal Solvation Model Based on Solute Electron Density and on a Continuum Model of the Solvent Defined by the Bulk Dielectric Constant and Atomic Surface Tensions. *J. Phys. Chem. B* **113**, 6378–6396 (2009).

58. Weigend, F. & Ahlrichs, R. Balanced basis sets of split valence, triple zeta valence and quadruple zeta valence quality for H to Rn: Design and assessment of accuracy. *Phys. Chem. Chem. Phys.* **7**, 3297 (2005).

59. Weigend, F. Accurate Coulomb-fitting basis sets for H to Rn. *Phys. Chem. Chem. Phys.* **8**, 1057 (2006).

Supplementary Information

This file contains detailed methods with relevant data, figures, and tables.

Acknowledgements

We are grateful for Dr. I. Keresztes for acquiring 2D NOESY and 2D HMBC NMR spectra and providing guidance, insights, and discussions regarding NMR analyses. We thank Prof. D. Collum and Dr. Q. You for use of the React IR. We thank Prof. R. Cerione and Dr. S. Milano for the use of the pH meter. We thank B. Ahmad for helping with designing the flue gas dosing setup. We thank Dr. R. Siegelman for helpful feedback. We thank the Cornell Heat and Power (CHP) plant for donating a sample of flue gas. This work made use of the Bard Materials and Characterization facility of the Cornell Center for Materials Research (CCMR).

Funding: This work was supported by a Research-to-Impact Fast Grant awarded by the 2030 Project and the Cornell Atkinson Center for Sustainability (S.M., T.H.L., P.J.M.). This work was also supported by the Carbontech Development Initiative (S.M., T.H.L., P.J.M.). This work was further supported by the U.S. Department of Energy, Office of Science, Office of Basic Energy Sciences under Award Number DE-SC0021000 (S.M., P.J.M.). We also acknowledge support from a Camille Dreyfus Teacher-Scholar Award to P.J.M. (TC-23-048). The NMR data were collected on a Bruker AV III HD 500 MHz spectrometer that was purchased with support from the National Science Foundation (CHE-1531632).

Author contributions: S.M. carried out NMR studies, IR studies, gravimetric measurements, pH measurements, viscosity measurements, and DFT calculations. S.M. wrote the original draft with editorial assistance from P.J.M. and T.H.L.. P.J.M. and T.H.L. directed the research.

Competing interests: Cornell University has filed a provisional patent application related to this work on which S.M., P.J.M., and T.H.L. are included as inventors.